Proceedings of the 3rd International Conference on Environmental Geoscience and Earth Ecology
DOI: 10.54254/2753-8818/2025.24543

# *DFT Study on the $NH_3$-SCR Denitration Mechanism Catalyzed by Ce Active Sites in Fluorocarbonatite*

**Zhaoyang Meng[1], Kai Zhang[1*]**

*School of Energy and Environment, Inner Mongolia University of Science & Technology, Baotou, China*
**Corresponding Author. Email: btzk@imust.edu.cn*

***Abstract.*** Efficient removal of nitrogen oxides ($NO_x$) is one of the key tasks in atmospheric pollution control. Ammonia selective catalytic reduction ($NH_3$-SCR) technology has emerged as the mainstream denitration method due to its high efficiency and environmental friendliness, with catalyst design and performance optimization at its core. Traditional vanadium-based catalysts are gradually being phased out due to their high toxicity and narrow temperature window. In contrast, Fe-Ce synergistic catalytic systems have become the focus of next-generation denitration materials owing to their wide temperature activity range, high $N_2$ selectivity, and environmental compatibility. In this study, density functional theory (DFT) calculations are employed to systematically reveal the synergistic mechanism of Ce active sites in Fe-$CeCO_3F$ catalysts, elucidating their central role in optimizing the reaction pathway.

***Keywords:*** Fe-$CeCO_3F$, Ce active sites, $NH_3$-SCR, Density Functional Theory, Catalytic Reduction

## 1. Introduction

As one of the primary atmospheric pollutants, nitrogen oxides (NOx) have become a core issue in global environmental governance. While natural sources of NOx—such as volcanic activity and microbial decomposition—can be balanced through the self-purifying capacity of the environment, anthropogenic activities, including fossil fuel combustion, industrial emissions, and vehicle exhaust, have caused a dramatic increase in NOx concentration. This has led to severe environmental and public health problems. NOx can directly irritate the respiratory system, triggering respiratory diseases, and it participates in photochemical reactions that produce ozone and secondary aerosols, intensifying photochemical smog and PM2.5 pollution. Furthermore, NOx can be converted into nitric acid in the atmosphere, contributing to a shift in acid rain composition from a sulfuric to a mixed sulfuric-nitric type. According to 2020 statistics, China's annual NOx emissions exceeded 10 million tons, over 90% of which originated from stationary source flue gases and mobile source exhaust. Notably, nitrates have surpassed sulfates in their proportion of PM2.5, becoming one of the main components of haze. Against this backdrop, developing efficient NOx reduction technologies has become an urgent necessity [1].

DOI: 10.54254/2753-8818/2025.24543

Selective catalytic reduction using ammonia ($NH_3$-SCR) is regarded as a key solution to NOx pollution due to its high denitrification efficiency and mature industrial application [2]. This technique employs $NH_3$ as a reducing agent to convert NOx into harmless $N_2$ and $H_2O$ over a catalyst surface. Although traditional vanadium-based catalysts (e.g., $V_2O_5$-$WO_3$/$TiO_2$) perform well at high temperatures (300–400°C), their narrow active temperature window, high toxicity, and poor low-temperature activity limit their ability to meet increasingly stringent environmental regulations [3]. In recent years, rare-earth-based catalysts have emerged as research hotspots in the low-temperature $NH_3$-SCR field, owing to their unique redox properties and tunable structures. Among them, cerium (Ce)-based materials have attracted significant attention for their reversible $Ce^{3+}/Ce^{4+}$ redox pairs, excellent oxygen storage capacity, and environmental compatibility [4]. Studies have shown that cerium-based materials such as $CeO_2$ can facilitate NO oxidation to highly reactive $NO_2$ via surface oxygen vacancies and enhance $NH_3$ adsorption and activation through Lewis acid sites [5]. However, monometallic Ce-based catalysts still suffer from low activity at temperatures below 200°C and poor resistance to sulfur and water, which restrict their practical applications [6].

To make progress in this field, researchers have explored the incorporation of transition metals (e.g., Fe, Mn, Cu) to construct multi-metallic synergistic catalytic systems [7]. Among them, iron (Fe) has emerged as an ideal candidate due to its rich d-orbital electrons, variable oxidation states ($Fe^{2+}/Fe^{3+}$), and low cost [8]. Experimental evidence indicates that Fe-Ce composite catalysts exhibit significantly higher denitrification efficiency across a wide temperature range (150–400°C) than single-component counterparts. For instance, Fe-doped $CeO_2$ catalysts can achieve NOx conversion rates above 90% at 250°C and maintain stable activity even under coexisting water vapor and $SO_2$ conditions [9]. This synergistic effect arises from the complementary functions of Fe and Ce: Ce dynamically regulates the adsorption and diffusion of reactants via oxygen vacancies, while Fe accelerates the generation of key intermediates (e.g., $NH_2$, $NO_2$) through redox cycling [10]. However, most current studies focus on macroscopic performance optimization, with limited in-depth analysis of the atomic-level synergy between Fe and Ce—such as electron transfer pathways, interfacial orbital hybridization, and oxygen vacancy formation mechanisms. As a result, catalyst design remains stagnant, and breakthroughs from macro to micro levels are difficult to achieve.

The Bayan Obo mining area in Inner Mongolia, the world's largest light rare earth deposit, provides a unique resource advantage for developing high-efficiency low-temperature denitrification catalysts [11]. This region accounts for 81% of China's total rare earth reserves, with light rare earth minerals such as bastnaesite ($CeCO_3F$) and monazite comprising over 95% of the deposits. These minerals naturally coexist with transition metals such as Fe and Mn. Notably, bastnaesite is not a single-component system; $Ce^{3+}$ in its crystal structure often undergoes isomorphous substitution with $Fe^{2+}$ and $Mn^{2+}$ to form multi-metallic coexisting active sites [12]. Such naturally occurring mineral structures may function catalytically through the following mechanisms: (1) $Ce^{3+}/Ce^{4+}$ redox pairs and $Fe^{2+}/Fe^{3+}$ cycles form synergistic charge transfer pathways that enhance redox capabilities; (2) Fe doping induces lattice distortion and increases surface oxygen vacancy concentrations, thereby optimizing NO adsorption and activation; (3) the coordination environments of $CO_3^{2-}$ and $F^-$ in the mineral modulate surface acidity and basicity, strengthening $NH_3$ adsorption and dissociation. However, the complex intergrowth structures and impurity interference in natural minerals make it difficult to precisely control active sites, and the underlying mechanisms remain poorly understood. Most existing studies use mechanical mixing or simple impregnation to modify minerals, which can improve denitrification performance but fail to reveal the fundamental rules governing multi-metal synergy.

DOI: 10.54254/2753-8818/2025.24543

To address this issue, the key to high-value utilization of Bayan Obo rare earth resources lies in a "biomimetic design" approach—that is, artificially synthesizing structures that mimic bastnaesite crystals while incorporating transition metal dopants directionally to construct model catalysts with active sites closely resembling those of natural minerals. For example, using $CeCO_3F$ as the base and substituting part of the Ce sites with Fe atoms [13] allows precise tuning of surface oxygen vacancy concentration and distribution; sulfuric acid pretreatment can expose more Brønsted acid sites, enhancing $NH_3$ adsorption strength [14]. This strategy of "structural biomimicry + compositional tuning" not only preserves the cooperative advantages of natural minerals but also eliminates impurity interference through controllable modifications, offering an ideal platform for mechanistic studies. However, a major challenge in this direction remains unresolved: the electron transfer mechanism at the Fe-Ce interface and the dynamic evolution of reaction intermediates are still unclear, hindering the establishment of a quantitative relationship between composition, structure, and performance.

To address these challenges, this study takes Bayan Obo bastnaesite as a prototype and constructs a Fe-doped Fe-$CeCO_3F$ model catalyst. It investigates in detail the surface redox sites, acid-base active centers, and multi-metal synergistic effects. Using density functional theory (DFT) calculations, the study elucidates the cooperative mechanism of Ce sites in both Eley-Rideal (E-R) and Langmuir-Hinshelwood (L-H) reaction pathways.

## 2. Calculation methods

### 2.1. Crystal plane calculation

As shown in Figure 1, based on the $CeCO_3F$ PDF#11-0340 reference card, the most frequently exposed crystal planes of $CeCO_3F$ are (110) and (112). Additionally, literature review indicates that the (100) plane is also a commonly exposed cleavage plane. Therefore, the (100) plane is selected for subsequent calculations.

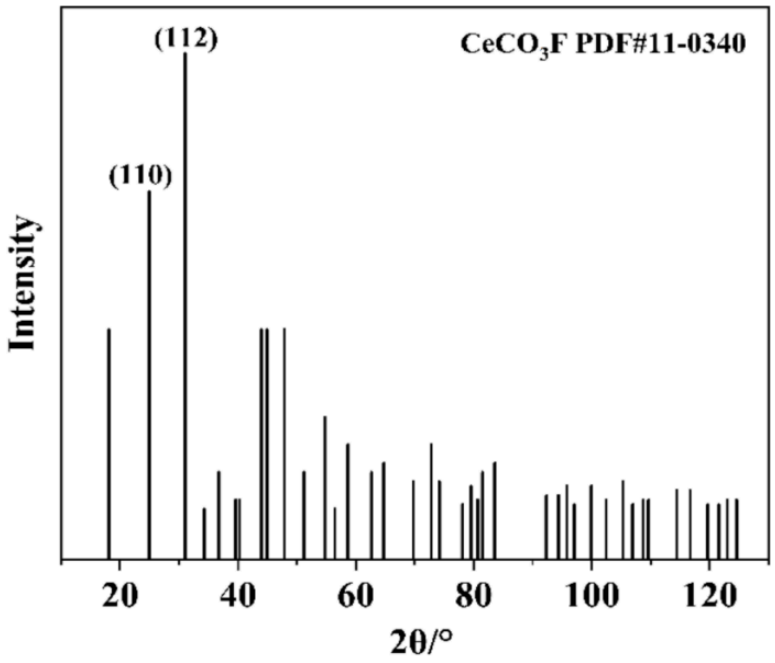


Figure 1: $CeCO_3F$ PDF#11-0340 reference card

DOI: 10.54254/2753-8818/2025.24543

## 2.2. Atomic radius calculation

The covalent and van der Waals radii of the atoms involved in the calculations are listed in Table 1. When chemical bonds form, the bond length is generally close to the sum of the covalent radii of the two atoms. Compared to covalent radii, cationic radii are significantly smaller, while anionic radii are noticeably larger. The sum of ionic radii aligns well with the interionic distance, making it unnecessary to consider ionic radii separately. Under equilibrium conditions, if the primary interaction between atoms is van der Waals forces, their distance usually approximates the sum of their respective van der Waals radii. When non-covalent interactions such as hydrogen bonds, halogen bonds, or π–π stacking exhibit strong intensities, the interatomic distances become significantly shorter than conventional van der Waals distances. In such cases, it can be said that the atoms have surpassed the boundary imposed by van der Waals forces, as if penetrating each other's van der Waals surfaces. When the sum of the van der Waals radii of two atoms is exceeded, the interaction between them is generally considered weak and negligible.

Table 1: Covalent and van der Waals radii of atoms (R/Å)

| R | H | C | N | O | F | Fe | Ce |
|---|---|---|---|---|---|---|---|
| Covalent Radius | 0.31 | 0.76 | 0.71 | 0.66 | 0.57 | 1.39 | 2.04 |
| Van der Waals Radius | 1.08 | 1.49 | 1.41 | 1.4 | 1.39 | 2.05 | 2.42 |

## 2.3. Transition state calculations

Transition state calculations, formally known as the Nudged Elastic Band (NEB) method, serve as a critical theoretical tool aimed at locating saddle points on the potential energy surface between reactants and products, as well as identifying the minimum energy reaction pathway. The key feature of this method is the manipulation of a series of intermediate images to investigate the system's kinetic properties. Each image is optimized to find its lowest energy configuration while maintaining a fixed distance from adjacent images. This constrained optimization process uses spring forces to link the images and compute forces projected along and perpendicular to the reaction pathway, thereby enabling effective treatment. An advancement of this method, the Climbing Image Nudged Elastic Band (CINEB), further enhances the approach by guiding the highest-energy image to converge precisely at the saddle point. In this procedure, the climbing image is no longer subject to spring forces but instead experiences a real force in the reverse direction along the tangent. The algorithm aims to maximize the energy along this path direction while minimizing it in all others, ensuring convergence exactly at the saddle point.

DOI: 10.54254/2753-8818/2025.24543

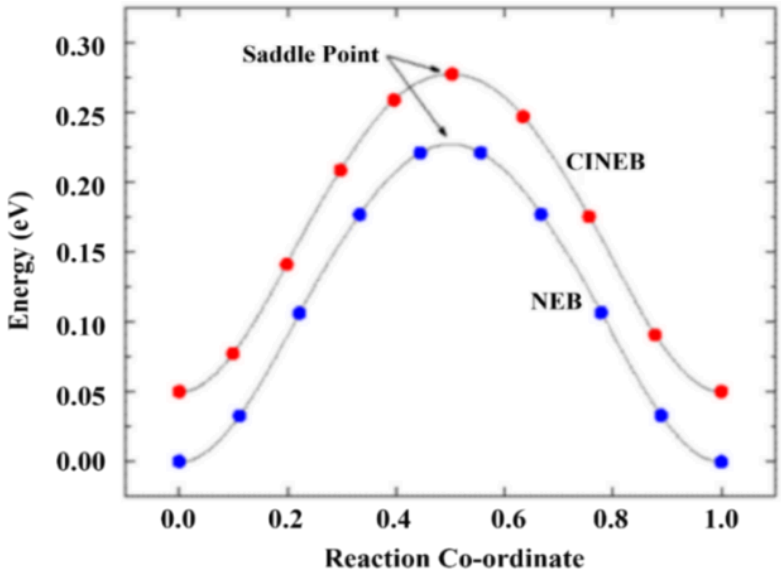


Figure 2: NEB and CINEB methods in transition state theory. Blue dotted line—NEB calculations; red dotted line—CINEB calculations

In this study, the transition states and intermediate products of the reaction were calculated using the CINEB method implemented in the VASP-VTST package. Initial guesses for the initial and final state structures were first optimized. Upon completion of the optimization, the lowest energy configuration of each intermediate was obtained. Linear interpolation was then performed between the initial and final states, and the interpolated structures were optimized. After convergence, the results were processed to locate the saddle point, which corresponds to the reaction transition state. The reaction energy ($\triangle E_r$) and energy barrier (Eba, also referred to as activation energy) for each reaction step were calculated using the following formulas:

$$\triangle E_r = E_F\, E_{IS} \tag{1}$$

$$E_{ba} = E_{TS}\, E_{IS} \tag{2}$$

In chemical kinetics, $E_{IS}$ denotes the energy of the initial state, $E_{TS}$ refers to the energy of the transition state, and $E_{FS}$ corresponds to the energy of the final state. Similar to the concept of adsorption energy, a negative value of $\triangle E_r$ indicates an exothermic reaction, which tends to release energy, while a positive value reveals the characteristics of an endothermic reaction. The formula for calculating adsorption energy will be presented in subsequent calculation sections.

## 3. System modeling

During the model construction process, as shown in Figure 3, a surface model of Fe–$CeCO_3F$ was obtained by substituting a surface Ce atom with an Fe atom. The model features three periodically arranged atomic layers. A vacuum layer of 15 Å was applied in the direction perpendicular to the crystal plane to eliminate interactions along the z-axis due to periodicity. As illustrated in the figure, doping results in shortened Fe–O and Fe–F bonds, rendering the structure more compact. During structural optimization, the upper one-third of the atomic layers was allowed to relax, while the bottom two-thirds were fixed. The core calculations were performed using the Vienna Ab-initio

DOI: 10.54254/2753-8818/2025.24543

Simulation Package (VASP), characterized by the Generalized Gradient Approximation (GGA) and the Perdew-Burke-Ernzerhof (PBE) functional. Computational parameters were appropriately configured to optimize efficiency. The Kohn–Sham equations were numerically solved using a plane-wave basis set and a self-consistent iteration algorithm, both based on the GGA. All simulations were conducted using the Effective Core Potential (ECP) method. The calculated lattice parameters were a = 14.3003 Å, b = 19.6540 Å, and c = 19.7366 Å. A 2 × 1 × 1 k-point grid was applied to sample the Brillouin zone. The +U approach was employed for the Ce 4f and Fe 3d orbitals, with a U value set to 4.5 eV. During structural optimization, the energy cutoff was set to 440 eV, and the convergence criteria for energy and force were set to $10^{-4}$ eV and –0.05 eV, respectively.

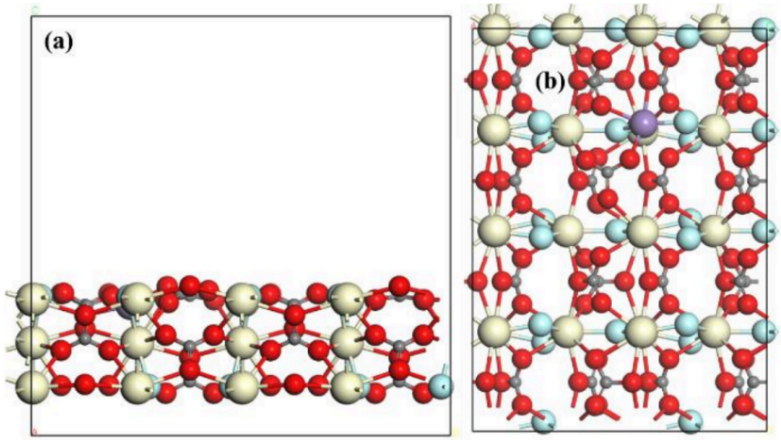


Figure 3: Fe-doped $CeCO_3F$ (100) crystal plane: (a) Front view; (b) Top view

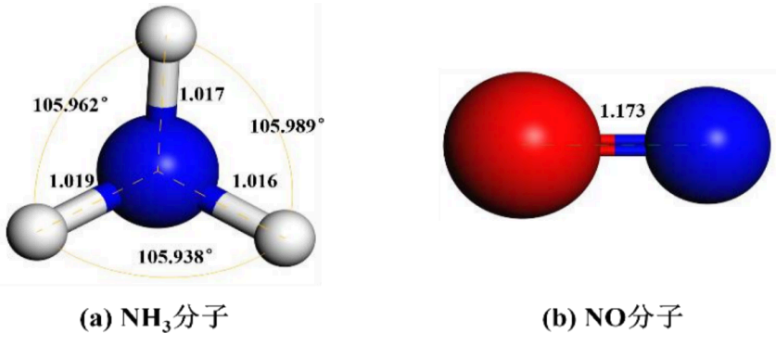


Figure 4: Optimized models of (a) $NH_3$ and (b) NO molecules. Blue: N; White: H

## 4. The core role and synergistic mechanism of Ce-based active sites in doping

### 4.1. Analysis of Ce-based reaction pathway

$$NH_3(g)+NO(g/*) \rightarrow N_2+H_2O+H* \quad (3)$$

The complete reaction process for $NH_3$-SCR can be described by the following equations:

$$Ce^{3+}+NH_3 \rightarrow Ce^{4+}\text{-}NH_3* \quad (4)$$

$$Ce^{4+}\text{-}NH_3* \rightarrow Ce^{4+}\text{-}NH_2*+H* \quad (5)$$

DOI: 10.54254/2753-8818/2025.24543

$$-NH_2^* + NO(g/^*) \rightarrow -NH_2NO^* \quad (6)$$

$$-NH_2NO^* \rightarrow -HNNOH^* \quad (7)$$

$$-HNNOH^* \rightarrow N_2 + H_2O \quad (8)$$

From the perspective of the electronic structure of Ce and its $NH_3$ adsorption properties, the empty orbitals of $Ce^{3+}$ form coordination bonds with the lone pair electrons of $NH_3$, enabling strong adsorption of $NH_3$ (Equation 4). The high oxidation state of $Ce^{4+}$ promotes the dehydrogenation of $NH_3$, generating the active species $-NH_2^*$ (Equation 5). At Lewis acid sites, the Lewis acidity of $Ce^{3+}$ enhances $NH_3$ adsorption stability through surface oxygen vacancies (IM1 structure in Figure 5). Meanwhile, the redox cycling of Ce drives $NH_3$ activation: during the oxidation of $Ce^{3+}$ to $Ce^{4+}$, $NH_3$ adsorption triggers the formation of a $Ce^{4+}$-$NH_3^*$ intermediate (Equation 4). DFT calculations show an adsorption energy of 0.47 eV for this step, indicating strong chemisorption (see the potential energy profile in Figure 6). The generation of $NH_2^*$ is accompanied by the reduction of $Ce^{4+}$ back to $Ce^{3+}$ (Equation 5), maintaining the catalytic cycle (IM2 → IM3 in Figure 5).

## 4.2. Mechanism analysis

1. In the Fe-Ce bimetallic catalyst system, Ce-based active sites play a central role in $NH_3$ adsorption and activation due to their unique redox properties ($Ce^{3+}/Ce^{4+}$ cycling) and strong Lewis acidity. With reference to the structural diagrams (Figures 5 and 7) and energy profiles (Figures 6 and 8), this section focuses on the key role of Ce in both the Eley-Rideal (E-R) and Langmuir-Hinshelwood (L-H) mechanisms, as well as its synergistic interaction with Fe.

2. Role of Ce Active Sites and Reaction Pathways in the E-R Mechanism

The hallmark of the E-R mechanism is the direct reaction between a gaseous reactant and an adsorbed species, without requiring all reactants to be pre-adsorbed. In the Fe-Ce catalyst, Ce sites dominate $NH_3$ adsorption and activation, while Fe sites promote NO oxidation via radical generation. Figure 5 illustrates the evolution of intermediates under the E-R mechanism. Based on Equations 5 to 3.6, the detailed pathway is as follows:

(1) Adsorption of $NH_3$ and Oxidation of $Ce^{3+}$

$NH_3$ molecules are adsorbed onto $Ce^{3+}$ Lewis acid sites, where the lone pair electrons form a coordination bond with $Ce^{3+}$'s empty orbitals, generating a $Ce^{4+}$-$NH_3^*$ intermediate (Equation 4). This step is accompanied by the oxidation of $Ce^{3+}$ (IM1 structure in Figure 5). DFT calculations indicate an adsorption energy of 0.47 eV, confirming strong chemisorption at Ce sites.

(2) Dehydrogenation of $NH_3$ to Form Active $-NH_2^*$

The strong oxidizing nature of $Ce^{4+}$ facilitates the removal of a hydrogen atom from $NH_3$, forming $Ce^{4+}$-$NH_2$ and H (Equation 5). The potential energy diagram in Figure 6 shows that the activation barrier for the transition state TS1 is 1.638 eV, suggesting that the redox cycling of Ce significantly lowers the dehydrogenation activation energy. The resulting $-NH_2^*$ species is highly reactive and crucial for the subsequent reaction with NO.

(3) Direct Reaction Between Gaseous NO and $-NH_2^*$

Under the E-R mechanism, gaseous NO reacts directly with $-NH_2^*$ at the Ce site, forming an $-NH_2NO$ intermediate (Equation 6). The IM3 → IM4 transition in Figure 5 shows the NO molecule bonding with the N atom of $-NH_2^*$ via the N–O bond. The energy profile in Figure 6 reflects the reaction progression under low-temperature conditions.

(4) Intermediate Transformation and $N_2$ Formation

DOI: 10.54254/2753-8818/2025.24543

The -$NH_2NO$ intermediate undergoes intramolecular rearrangement to form -HNNOH (Equation 7), which finally decomposes into $N_2$ and $H_2O$ (Equation 8). The energy barriers for TS3 and TS4 are 1.500 eV and 2.029 eV, respectively. Fe sites further reduce the energy barrier by facilitating proton transfer, accelerating intermediate decomposition. The final product $N_2$ shows high selectivity, benefiting from the directional regulation of intermediates by Ce sites.

(5) Core Contributions of Ce in the E-R Mechanism

Redox Dynamic Equilibrium: The $Ce^{3+}/Ce^{4+}$ cycle not only drives $NH_3$ dehydrogenation but also sustains catalytic activity through rapid reduction (IM2 → IM3).

Interfacial Synergy: -$NH_2$* at Ce sites reacts directly with $NO_2$ generated by Fe sites at the interface, reducing the activation energy and forming the dominant pathway for low-temperature denitrification.

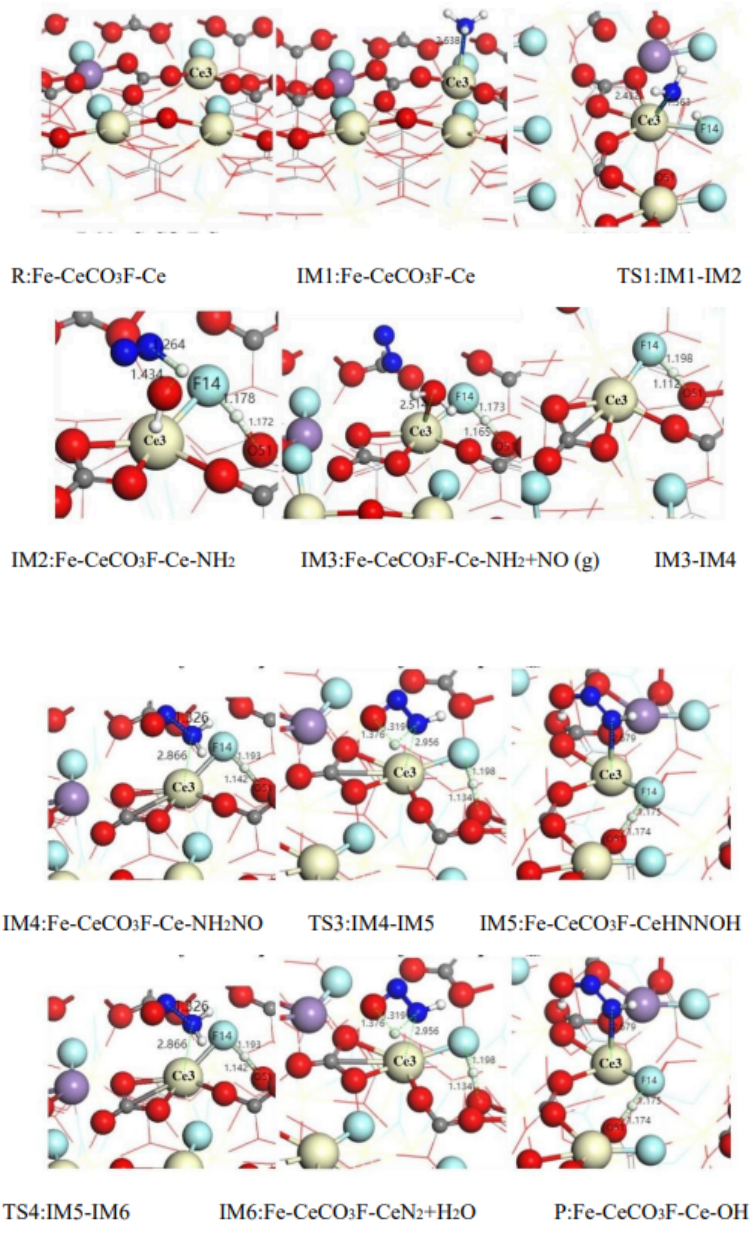


Figure 5: Structural diagrams of intermediates along the reaction pathway following the Eley-Rideal (E-R) mechanism at the Fe-$CeCO_3F$-Ce site

DOI: 10.54254/2753-8818/2025.24543

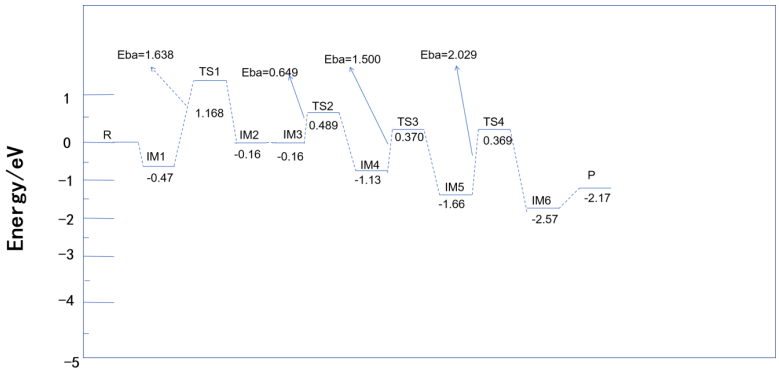


Figure 6: Potential energy diagram of the reaction pathway following the Eley-Rideal (E-R) mechanism at the Fe-$CeCO_3F$-Ce site

3. Adsorption Characteristics of Ce and Surface Reaction Limitations in the L-H Mechanism

The Langmuir–Hinshelwood (L-H) mechanism requires all reactants to be pre-adsorbed on the catalyst surface, and its reaction rate is limited by the surface mobility of the adsorbed species. Figure 7 illustrates the intermediate structures along the L-H pathway. Combined with the potential energy diagram (Figure 8), the analysis is as follows:

(1) Co-adsorption of $NH_3$ and NO

$NH_3$ preferentially adsorbs at the Ce site to form $Ce^{4+}$–$NH_2$*, while NO adsorbs at the Fe site to form $Fe^{3+}$–NO* (IM2 in Figure 7). This step requires overcoming an adsorption energy barrier of 1.638 eV (TS1 in Figure 8), resulting in a lower reaction rate at low temperatures compared to the Eley–Rideal (E-R) pathway.

(2) Surface Migration and Formation of –$NH_2NO$*

The adsorbed –$NH_2$ species must migrate to the Fe site to combine with NO and form –$NH_2NO$* (Equation 6). The energy barrier of TS2 in Figure 8 is 2.020 eV, indicating that surface diffusion is the rate-determining step. At elevated temperatures, the migration rate of adsorbed species increases, enabling the L-H pathway to approach the efficiency of the E-R mechanism. However, at low temperatures, the efficiency of this pathway is reduced, limiting its applicability.

(3) Common Features in Intermediate Decomposition Pathways

The subsequent steps of the L-H pathway (–$NH_2NO$* → –HNNOH* → $N_2$ + $H_2O$) are consistent with those in the E-R mechanism (Equations 3.5–3.6), though the overall potential energy surface is higher. OH* radicals at the Fe site accelerate the decomposition of –HNNOH* through proton transfer, partially offsetting the energy disadvantage.

DOI: 10.54254/2753-8818/2025.24543

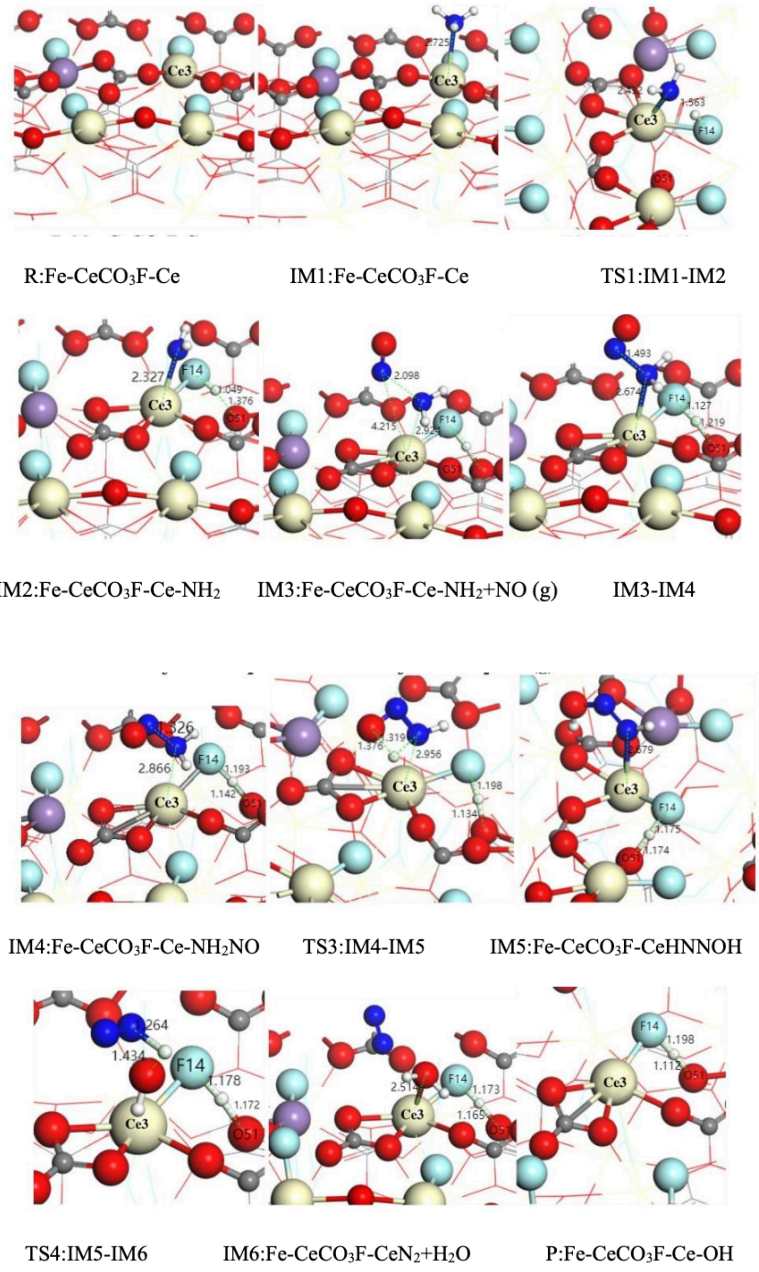


Figure 7: Structural diagrams of intermediates along the reaction pathway following the L-H (Langmuir–Hinshelwood) mechanism at the Fe–$CeCO_3F$–Ce site

DOI: 10.54254/2753-8818/2025.24543

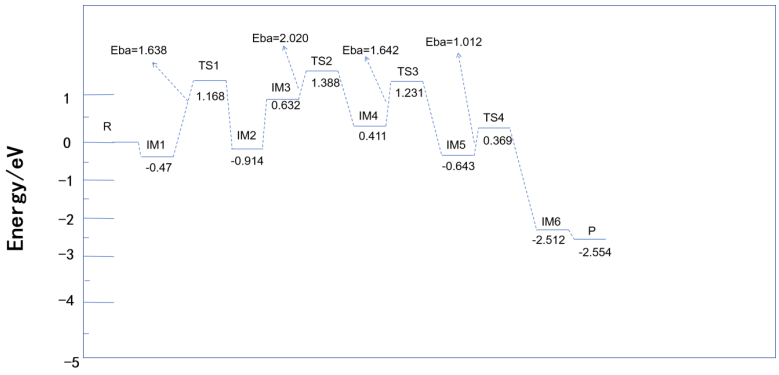


Figure 8: Potential energy diagram of the reaction pathway following the L-H (Langmuir–Hinshelwood) mechanism at the Fe–$CeCO_3F$–Ce site

## 5. Conclusion

This study investigated the reaction mechanism involving Ce sites on the Fe–$CeCO_3F$ surface and yielded the following conclusions:

Although the E-R and L-H mechanisms differ in their reaction pathways, the catalytic activity at Ce sites facilitates mutual complementation and synergistic enhancement between the two.

The initial stage is dominated by the E-R mechanism. Due to the absence of NO adsorption, the E-R pathway shows a significant advantage: $–NH_2$ at the Ce site reacts directly with $NO_2$ generated at the Fe site, lowering the activation energy and improving denitration efficiency at low temperatures. The potential energy diagram in Figure 6 shows that the main reaction process involves the combination of NO and $–NH_2$. The oxidative capacity of Ce reduces the dehydrogenation barrier of $NH_3$, optimizing overall electron transfer and energy distribution.

In the intermediate stage, the L-H mechanism serves as a complement. As the adsorption capacity increases, the L-H pathway becomes active. Oxygen vacancies in Ce facilitate the storage and release of oxygen species (e.g., O*), promoting the oxidation of NO to $NO_2$ at the Fe site, which then reacts with $–NH_2$* at the Ce site.

$N_2$ selectivity is assured through dual mechanisms. In both the E-R and L-H pathways, the decomposition of the intermediate –HNNOH* predominantly yields $N_2$ (Equation 8). The strong Lewis acidity of Ce stabilizes the reaction intermediates and suppresses the formation of byproducts such as $N_2O$.

## References

[1] Xiao, T. (2024). Assessment of air pollutant reduction measures and preliminary study on synergistic benefits of carbon reduction in resource-based cities of Shanxi Province (Master's thesis). Chinese Research Academy of Environmental Sciences. https: //doi.org/10.27510/d.cnki.gzhky.2024.000012

[2] Cheng, T., Jiang, Z., Hu, Y., Qin, K., Wu, W., Xie, Q., & Zhu, C. (2024). $TiO_2$ modified limonite for selective catalytic reduction of NO from cement kiln flue gas with $NH_3$. Molecular Catalysis, 561, 114191, ISSN 2468-8231.

[3] Dong, H., Gao, X., Zhu, J., Xiong, B., He, H., Ouyang, M., He, G., Li, H., & Lin, Z. (2025). What's next for batteries: A radical rethink of battery technology development for transportation and grid applications. Materials Today Energy, 50, 101864, ISSN2468-6069.

[4] Gao, C., Xiao, B., Shi, J.-W., He, C., Wang, B., Ma, D., Cheng, Y., & Niu, C. (2019). Comprehensive understanding the promoting effect of Dy-doping on MnFeOx nanowires for the low-temperature $NH_3$-SCR of NOx: An experimental and theoretical study. Journal of Catalysis, 380, 55–67, ISSN 0021-9517.

[5] Gao, H., Song, Z., Mao, Y., Fan, Y., Li, R., Chen, X., Liu, W., Zhang, J., Huang, Z., & Zhang, X. (2025). Tight coupling of oxygen vacancies and acidity on α-$MnO_2$ through cerium doping engineering for efficient removal of

DOI: 10.54254/2753-8818/2025.24543

multi-component VOCs. Applied Catalysis B: Environmental and Energy, 362, 124745, ISSN 0926-3373.
[6] Song, K., Feng, X., Zhang, N., Ma, D., Shi, L., Chen, Y., Li, J., & Shi, J.-W. (2025). Metal-organic framework materials in $NH_3$-SCR: Progress and prospects. Coordination Chemistry Reviews, 535, 216615, ISSN 0010-8545.
[7] Ali, H., Orooji, Y., Ajmal, Z., Abboud, M., Abu-Dief, A. M., Abu Al-Ola, K. A., Hassan, H. M. A., Yue, D., Guo, S.-R., & Hayat, A. (2025). A comprehensive review based on the synthesis, properties, morphology, functionalization, and potential applications of transition metals nitrides. Coordination Chemistry Reviews, 526, 216353, ISSN 0010-8545.
[8] Fan, Z., Wan, H., Yu, H., & Ge, J. (2023). Rational design of Fe-M-N-C based dual-atom catalysts for oxygen reduction electrocatalysis. Chinese Journal of Catalysis, 54, 56–87, ISSN 1872-2067.
[9] Wei, Y., & Li, Y. (2025). Low-temperature efficient catalytic oxidation of acetonitrile over Cu and Ce co-doped perovskite-type $LaMnO_3$ catalyst. Applied Catalysis A: General, 699, 120250, ISSN 0926-860X.
[10] Teng, X., Si, D., Chen, L., & Shi, J. (2024). Synergetic catalytic effects by strong metal–support interaction for efficient electrocatalysis. eScience, 4(6), 100272, ISSN 2667-1417.
[11] King, A. H., Eggert, R. G., & Gschneidner, K. A. (2016). The rare earths as critical materials. In J.-C. G. Bünzli & V. K. Pecharsky (Eds.), Handbook on the Physics and Chemistry of Rare Earths (Vol. 50, pp. 19–46). Elsevier, ISSN 0168-1273, ISBN 9780444638519.
[12] Pang, Y., Zheng, X., Wu, S., Wang, F., Shen, Z., & Chen, H. (2024). Bimetallic and multimetallic MOFs and their derivatives. In C. Guan (Ed.), Metal-organic frameworks and their derivatives for energy conversion and storage (pp. 37–62). Elsevier, ISBN 9780443188473.
[13] Cao, D., Tie, M., Zhang, G., & Huang, X. (2025). Research progress of Ce-based electrocatalysts in hydrogen evolution reaction. Journal of Rare Earths, ISSN 1002-0721.
[14] Liu, S., Gao, J., Xu, W., Ji, Y., Zhu, T., Xu, G., Zhong, Z., & Su, F. (2024). Transition metal-based catalysts for selective catalytic reduction of NO by CO: A state-of-the-art review. Chemical Engineering Journal, 486, 150285, ISSN 1385-8947.